Title

A novel function for the Caenorhabditis elegans torsin OOC-5 in nucleoporin localization and nuclear import.

Journal

Molecular biology of the cell, 26(9)

ISSN

1059-1524

Authors

VanGompel, Michael JW
Nguyen, Ken CQ
Hall, David H
et al.

Publication Date

2015-05-01

DOI

10.1091/mbc.e14-07-1239

Peer reviewed

A novel function for the *Caenorhabditis elegans* torsin OOC-5 in nucleoporin localization and nuclear import

Michael J. W. VanGompel[a], Ken C. Q. Nguyen[b], David H. Hall[b], William T. Dauer[c], and Lesilee S. Rose[a]

[a]Department of Molecular and Cellular Biology, University of California, Davis, Davis, CA 95616; [b]Center for *C. elegans* Anatomy, Albert Einstein College of Medicine, New York, NY 10461; [c]Departments of Neurology and Cell and Developmental Biology, University of Michigan Medical School, Ann Arbor, MI 48109

ABSTRACT **Torsin proteins are AAA+ ATPases that localize to the endoplasmic reticular/nuclear envelope (ER/NE) lumen. A mutation that markedly impairs torsinA function causes the CNS disorder DYT1 dystonia. Abnormalities of NE membranes have been linked to torsinA loss of function and the pathogenesis of DYT1 dystonia, leading us to investigate the role of the *Caenorhabditis elegans* torsinA homologue OOC-5 at the NE. We report a novel role for torsin in nuclear pore biology. In *ooc-5*–mutant germ cell nuclei, nucleoporins (Nups) were mislocalized in large plaques beginning at meiotic entry and persisted throughout meiosis. Moreover, the KASH protein ZYG-12 was mislocalized in *ooc-5* gonads. Nups were mislocalized in adult intestinal nuclei and in embryos from mutant mothers. EM analysis revealed vesicle-like structures in the perinuclear space of intestinal and germ cell nuclei, similar to defects reported in torsin-mutant flies and mice. Consistent with a functional disruption of Nups, *ooc-5*–mutant embryos displayed impaired nuclear import kinetics, although the nuclear pore-size exclusion barrier was maintained. Our data are the first to demonstrate a requirement for a torsin for normal Nup localization and function and suggest that these functions are likely conserved.**

Monitoring Editor
Martin Hetzer
Salk Institute for Biological Studies

Received: Jul 25, 2014
Revised: Feb 5, 2015
Accepted: Feb 24, 2015

INTRODUCTION

Torsins are AAA+ ATPases localized to the lumen of the endoplasmic reticulum (ER) and contiguous perinuclear space (Gerace, 2004; Cookson and Clarimon, 2005; Granata *et al.*, 2009). ATPases associated with a variety of cellular activities (AAA+ ATPases) use energy derived from ATP hydrolysis and often unfold misfolded proteins or disassemble protein complexes (Vale, 2000; Hanson and Whiteheart, 2005; Granata *et al.*, 2009). A mutation in the *TOR1A* gene that removes a single glutamic acid ("ΔE") from the torsinA protein causes DYT1 dystonia, a neurodevelopmental disease characterized by prolonged involuntary twisting movements (for review, see Tanabe *et al.*, 2009; Dauer, 2014).

Several studies indicate that the DYT1 mutation impairs torsinA function and implicate torsinA in ER protein quality control pathways and cellular stress responses. In *Caenorhabditis elegans*, overexpression of human torsinA reduced polyglutamine-induced protein aggregates (Caldwell *et al.*, 2003) and protected neurons from degeneration in the face of cellular stressors (Cao *et al.*, 2005). Of importance, ΔE-torsinA did not provide these protective effects. A similar protective effect was seen when ER stress was measured specifically (Chen *et al.*, 2010). Furthermore, a *C. elegans* torsin homologue, TOR-2, provided similar protective effects to torsinA, indicating conservation of these functions (Caldwell *et al.*, 2003; Cao *et al.*, 2005; Chen *et al.*, 2010). In cell culture, wild-type torsinA has also been implicated in ER-associated degradation (Nery *et al.*, 2011).

TorsinA localization to and interactions at the nuclear envelope (NE) have also been described. ATP-locked torsinA accumulates at the NE in cell culture, suggesting that torsin substrates are present

This article was published online ahead of print in MBoC in Press (http://www.molbiolcell.org/cgi/doi/10.1091/mbc.E14-07-1239) on March 4, 2015.

Address correspondence to: Michael VanGompel (mjwvangompel@ucdavis.edu), Lesilee Rose (lsrose@ucdavis.edu).

Abbreviations used: NPP, nuclear pore complex protein; OOC, oocyte defective.

at the NE (Gerace, 2004; Goodchild and Dauer, 2004; Naismith *et al.*, 2004). Indeed, torsinA interacts with the inner nuclear membrane (INM) protein LAP1, which is required for perinuclear accumulation of ATP-locked torsinA (Goodchild and Dauer, 2005). TorsinA also associates with the lumenal KASH domain of the outer nuclear membrane (ONM) protein nesprin (Gonzalez-Alegre and Paulson, 2004; Nery *et al.*, 2008). ONM KASH domain proteins interact with INM SUN-domain proteins to connect the cytoskeleton with the nucleoskeleton. Interestingly, SUN1 is required for NE accumulation of ΔE-torsinA (Jungwirth *et al.*, 2011), further supporting a connection between torsinA and SUN-KASH proteins. Similar to ATP-locked torsinA, ΔE-torsinA accumulates at the NE, and this accumulation alters the subcellular distribution of nesprin proteins (Nery *et al.*, 2008), suggesting that NE-associated functions could be important to DYT1 dystonia. Animal models of torsins are consistent with this notion. Both torsinA null and homozygous ΔE-torsinA knock-in mice exhibit defects specifically in neuronal NE ultrastructure while ER structure is intact (Goodchild *et al.*, 2005). In addition, hypofunction of torsinA during neural development causes dystonic-like twisting movements in mice (Liang *et al.*, 2014), further connecting torsinA loss of function to dystonic movements. A NE structural defect similar to that observed in mice was seen in torsin-mutant flies (Jokhi *et al.*, 2013). These data demonstrate that the DYT1 mutation impairs torsinA function and suggest that a conserved role at the NE is disrupted in the pathogenesis of DYT1 dystonia.

Despite the clear relationship between torsinA and the NE, defects in nuclear pore complex (NPC) localization or function have not been examined. NPCs are made up of ~30 different proteins called nucleoporins (Nups) and maintain a diffusion barrier to large molecules while also mediating nuclear import and export (D'Angelo and Hetzer, 2008; Wente and Rout, 2010). TorsinA was implicated in a novel budding mechanism for the export of mega ribonucleoproteins (RNPs) directly through the NE, but this process is not believed to involve nuclear pores (Speese *et al.*, 2012; Jokhi *et al.*, 2013). Interestingly, RNA interference (RNAi) depletion of a subset of Nups in *C. elegans* leads to a phenotype similar to that observed in mutants for the torsin homologue oocyte defective-5 (OOC-5; Schetter *et al.*, 2006). Worms lacking either nuclear pore complex protein-1 (NPP-1; mammalian mNup54) or OOC-5 produce smaller-than-normal oocytes, and the subsequent embryos exhibit defects in cell polarity and asymmetric division. This suggests that the torsin OOC-5 may have a role at the nuclear pore or with a subset of nucleoporins. To explore this possibility, we analyzed nucleoporin localization and NPC function in *ooc-5* mutants and report a novel role for a torsin in Nup localization and nuclear import. We also observed NE ultrastructural defects similar to those reported in mammalian and *Drosophila* torsin mutants, demonstrating a conserved role for torsin proteins at the NE from worms to vertebrates.

RESULTS

Multiple nucleoporins are mislocalized in *ooc-5* germ cells

We first examined nucleoporin localization in *ooc-5(it145)*–mutant adults, using a NPP-9::green fluorescent protein (GFP; mammalian Nup 358/Ranbp2) reporter strain (Voronina and Seydoux, 2010). The *it145* allele (hereafter referred to as *ooc-5* for simplicity) has a nonsense mutation that truncates the protein before the ATPase domain and is a known strong loss-of-function mutation (Basham and Rose, 1999, 2001). NPP-9 is one of the Nups predominantly recognized by the widely used antibody Mab414 (Galy *et al.*, 2003; see later discussion) and is part of the cytoplasmic filament structure of the nuclear pore. We examined NPP-9::GFP in the germline, since defective oogenesis appears to be a primary defect in *ooc-5*–mutant worms. In addition, the *C. elegans* gonad contains nuclei in all stages of germ cell development, identifiable by their characteristic DNA morphology. These nuclei are organized in a spatiotemporal manner, allowing the developmental timing and progression of mutant phenotypes to be characterized in a single animal.

The *C. elegans* gonad is a U-shaped tube in which mitotic nuclei are located in the distal tip region (Figure 1A). Meiosis begins in the transition zone, followed by a pachytene region that extends throughout most of the distal gonad. At the loop of the gonad, germ cells enter diplotene and begin to grow, ultimately forming a single row of diakinesis oocytes in the proximal gonad, immediately adjacent to the spermatheca. In *ooc-5* young adult mutants, oocytes are ~60% of wild-type size and form a double or multiple row in the proximal gonad (Basham and Rose, 1999).

In control gonads, NPP-9::GFP localized to foci that were evenly distributed around the NE, referred to as "clusters" (Figure 1B; $N = 15$). This localization of Nups has been reported with Mab414 immunostaining, and ultrastructural analysis by electron microscopy (EM) confirmed the existence of clusters of NPCs in germ cell nuclei (Pitt *et al.*, 2000; Sheth *et al.*, 2010). In contrast, in *ooc-5* gonads, NPP-9::GFP localized to larger, flatter, unevenly spaced foci in *ooc-5* gonads, which we term "plaques" (Figure 1B). This abnormal localization became apparent in the transition zone and persisted through pachytene, diplotene, and diakinesis stages in all *ooc-5* worms ($N = 20$), often with multiple plaques present per nucleus (Figure 1, B and D).

We next asked whether these NPP-9::GFP plaques represented mislocalization of entire NPCs or only a subset of Nups. The components of the NPC are organized into structural subcomplexes including the inner scaffold, the nuclear basket, the cytoplasmic filament, the central plug, and transmembrane Nups. NPP-9 is a component of the cytoplasmic filament (mNup352/RanBP2; Voronina and Seydoux, 2010). We examined GFP Nup fusion reporters representing other subcomplexes (Figure 1C): NPP-1/mNup54 for the central plug (Schetter *et al.*, 2006; Golden *et al.*, 2009), NPP-19/mNup35 for the inner scaffold (Rodenas *et al.*, 2009), NPP-7/mNup153 for the nuclear basket (Voronina and Seydoux, 2010), and NPP-22/mNdc1 for transmembrane Nups (Stavru *et al.*, 2006). In control worms, localization of these reporters was similar to NPP-9::GFP, although the amount of rim signal and how distinct the clusters were varied among reporters (Figure 1C).

Similar to NPP-9::GFP, NPP-1::GFP formed abnormal plaques in all *ooc-5*–mutant worms. NPP-1::GFP plaques were first observed in the transition zone and persisted through diakinesis ($N = 15$). In contrast to NPP-9::GFP, continuous nuclear rim signal was still detectable between plaques of NPP-1::GFP, although this may result from different intensities of the GFP reporters. NPP-7::GFP and NPP-19::GFP also mislocalized in *ooc-5* germ cells ($N = 12$ germ lines each) but to a lesser extent than either NPP-1::GFP or NPP-9::GFP (Figure 1, C and D). That is, plaques of NPP-7::GFP or NPP-19::GFP were seen in late pachytene nuclei but not earlier. Further, only some pachytene nuclei had plaques (36/62 = 58% for NPP-7::GFP, 45/86 = 52% for NPP-19::GFP) compared with mislocalization of NPP-1::GFP and NPP-9::GFP in 100% of pachytene nuclei ($N = 60$ for both). In addition, among *ooc-5*–mutant pachytene nuclei with plaques, most nuclei had only one or two NPP-7::GFP or NPP-19::GFP plaques, whereas in the majority of nuclei, NPP-1::GFP and NPP-9::GFP were localized to three or more plaques (Figure 1D). NPP-22::GFP localization was examined after *ooc-5(RNAi)* (Figure 1C). Even in worms showing the strong *ooc-5* germline phenotype (see *Materials and Methods*), only some nuclei exhibited plaques (48/90 = 53%), and the majority

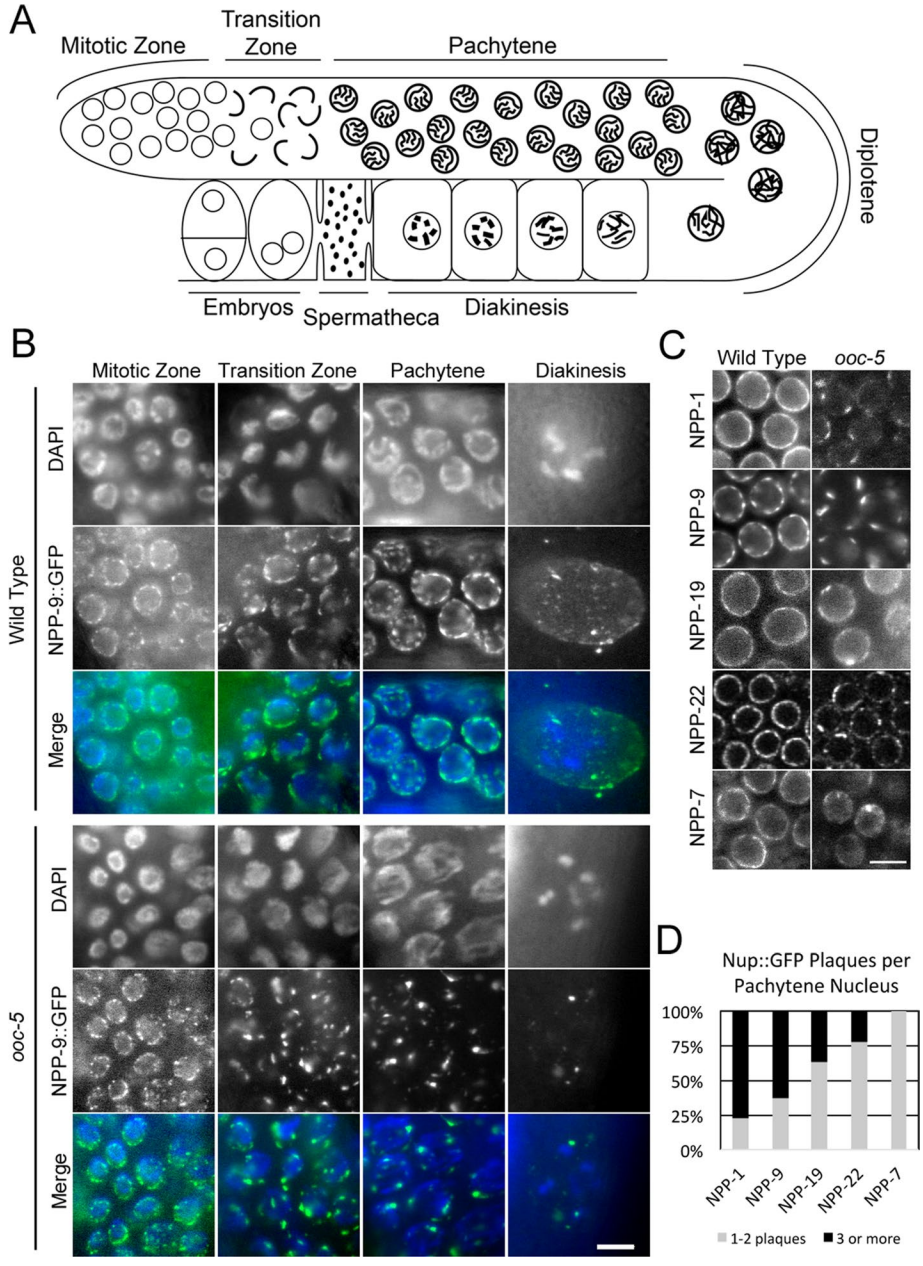

FIGURE 1: Nucleoporin defects in the *ooc-5* germline. (A) Schematic of the *C. elegans* germline. (B) Wide-field of images NPP-9::GFP–expressing worms fixed and stained for DAPI. (C) Pachytene nuclei from live worms expressing Nup reporters representing different parts of the NPC: NPP-1::GFP (mNup54), central channel; NPP-9::GFP(mNup358/RanBP2), cytoplasmic filament; NPP-19::GFP (mNup35), scaffold; NPP-22::GFP (mNdc1), transmembrane; and NPP-7::GFP (mNup153), nuclear basket. (D) Quantification of number of plaques of different reporters in *ooc-5* mutants. Scale bars, 5 μm.

of these nuclei had only one or two plaques (Figure 1D), similar to the results with NPP-7 and NPP-19.

Using Mab414 antibody, which recognizes FG-repeat Nups, including NPP-9 and NPP-10 (Davis and Blobel, 1987; Galy *et al.*, 2003), we observed large plaques in *ooc*-5 mutants, just as with the NPP-9::GFP reporter; this Mab414 mislocalization was similar in three different Nup::GFP reporter strains and in *ooc-5* mutants without a reporter. This indicates that overexpression of different Nup transgenes was not altering the Nup phenotypes (Supplemental Figure S1). Together these observations demonstrate that loss of OOC-5 function causes the mislocalization of nucleoporins from multiple subcomplexes but that outer Nups (NPP-9 and NPP-1) may be more severely mislocalized.

We next explored whether the mislocalized Nups colocalized in the plaques or were present in separate aggregates by staining NPP-9::GFP worms with Mab414. In control worms, NPP-9::GFP colocalized with Mab414 signal from the mitotic zone through the loop region (Figure 2A; four worms). In diakinesis oocytes of control worms, Mab414 staining was reduced at the NE and was instead found distributed throughout the cytoplasm, as previously reported (Pitt *et al.*, 2000). In contrast, NPP-9::GFP was primarily at the NE and there were fewer NPP-9::GFP foci observed in the cytoplasm; the cytoplasmic foci were predominantly separate from Mab414 foci, although some colocalization was observed. In *ooc-5* mutants, NPP-9::GFP and Mab414 colocalized throughout the gonad, including in diakinesis, where large plaques of NPP-9 and Mab414 colocalized both on the NE and in the cytoplasm (five worms).

In contrast to NPP-9::GFP, NPP-19 plaques did not fully colocalize with Mab414 in *ooc-5* germlines examined by double-antibody staining (Figure 2B). In *ooc-5* mutants, NPP-19 NE rims were less distinct than wild type, and plaques were prominent, similar to what was observed with the NPP-19::GFP reporter ($N = 4$). The NPP-19 plaques often colocalized with Mab414, although isolated Mab414 and NPP-19 punctae were also observed. Because Mab414 recognizes multiple Nups, we repeated NPP-19 staining in NPP-9::GFP–expressing worms to look specifically at the colocalization of these two Nups. We similarly observed that NPP-19 and NPP-9::GFP plaques sometimes colocalized but were also present at independent foci (Figure 2C; $N = 8$). These results show that Nups from different subcomplexes can colocalize in *ooc-5*–mutant germ cells but are sometimes present in distinct plaques.

The KASH protein ZYG-12 is mislocalized in *ooc-5* mutants

The mislocalization of multiple Nups in *ooc-5*–mutant germlines led us to test whether this reflected a more general defect in NE-associated protein organization. The NE has several classes of associated proteins, including lamins, LEM-domain INM proteins that associate with lamins, and transmembrane SUN and KASH domain proteins that together span the perinuclear space to form the linker of nucleoplasm and cytoplasm (LINC) complex (Gorjanacz *et al.*, 2007; Starr and Fridolfsson, 2010). In *ooc-5* mutants, the single *C. elegans* lamin, LMN-1, was localized in smooth circles at the NE throughout the gonad, similar to controls (Figure 3A; wild type, $N = 12$; *ooc-5*, $N = 10$). We next examined localization of the INM LEM-domain protein reporter LEM-2::GFP

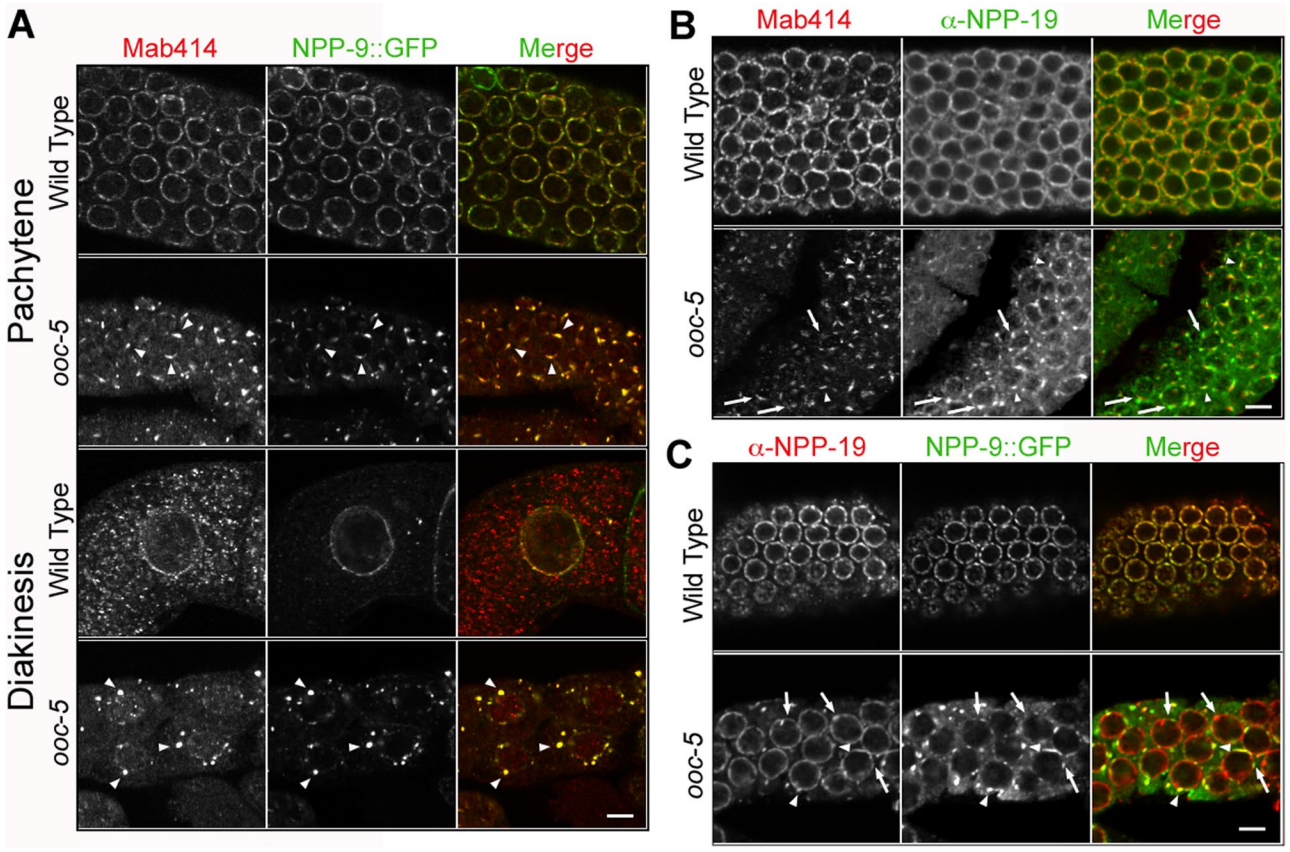

FIGURE 2: Colabeling of nucleoporins in the germline. Confocal sections of (A) Mab414 staining of NPP-9::GFP–expressing worms. (B) Double-antibody staining of wild-type and *ooc-5* gonads using anti–NPP-19 and Mab414. Both Mab414 and NPP-19 form plaques in *ooc-5* and sometimes (arrowhead) but not always (arrows) colocalize. (C) Anti–NPP-19 staining of NPP-9::GFP worms. NPP-19 and NPP-9::GFP sometimes (arrows) and sometimes do not (arrowheads) colocalize. Scale bars, 5 μm.

(Galy *et al.*, 2003). Although cytoplasmic signal was higher in *ooc-5*, the NE localization was localized normally to a smooth rim without plaques or gaps in pachytene through diakinesis germ cells (Figure 3A; wild type, $N = 18$; *ooc-5*, $N = 14$). This transgene signal was too faint to observe before pachytene. Together these data suggest that there is not a general disruption of NE proteins in *ooc-5*–mutant worms.

We next looked at the ONM KASH-domain protein ZYG-12 (Malone *et al.*, 2003). ZYG-12 is a germline-expressed homologue of nesprin proteins, which have been linked to wild-type and ΔE-torsinA in mammalian cell culture studies. In control worms, ZYG-12::GFP localized to a smooth rim in the mitotic zone and formed foci in the transition zone (Figure 3B; $N = 12$); these foci are associated with chromosome pairing centers important for homologous pairing (Penkner *et al.*, 2009; Sato *et al.*, 2009). After the transition zone, ZYG-12 relocalized to a smooth NE pattern (Figure 3B; Sato *et al.*, 2009). In *ooc-5* germlines, ZYG-12 localization appeared normal in the mitotic zone, formed foci in the transition zone, and relocalized to smooth rims in early pachytene nuclei (Figure 3B). However, as pachytene nuclei progressed toward the loop, discontinuities in ZYG-12::GFP were observed in *ooc-5* germlines (13 germlines, 54/72 nuclei); similar discontinuities were not observed in control worms (six germlines, 55 nuclei).

One possible explanation for the ZYG-12 discontinuities is that large Nup plaques prevent the localization of ZYG-12 on the NE. To test this hypothesis, we stained ZYG-12::GFP reporter worms with either Mab414 or NPP-19 antibody. Although Mab414 and NPP-19 plaques occasionally localized to areas lacking ZYG-12::GFP, Nup plaques were more often colocalized with regions where ZYG-12 remained in the NE (Figure 3, C and D; five germlines for Mab414, seven germlines for NPP-19). This indicates that discontinuities in ZYG-12 are not due to a physical exclusion by Nup plaques. Together these data show that OOC-5 is required for the normal localization of a subset of NE-associated proteins.

Nups are mislocalized in *ooc-5*–mutant intestinal and embryonic nuclei

OOC-5 protein is also present in embryos and adult intestinal tissue (Basham and Rose, 2001), although its full expression pattern has not been characterized. To determine whether Nups were also mislocalized in embryos from *ooc-5*–mutant mothers (hereafter called *ooc-5* embryos), we assessed Mab414 immunostaining and NPP-9::GFP fluorescence. In control embryos, Mab414 localized to a smooth rim at the NE (Figure 4A; $N = 5$; Galy *et al.*, 2003; Schetter *et al.*, 2006; Voronina and Seydoux, 2010). In *ooc-5* embryos, however, Mab414 punctae were seen at the NE (Figure 4A; $N = 4$). Similar to Mab414, NPP-9::GFP was mislocalized in *ooc*-5–mutant embryos ($N = 7$). The Nup mislocalization phenotypes observed in embryos appeared less severe than in *ooc-5*–mutant germlines but were similar to NPC phenotypes described after RNAi depletion of *npp-1*, *npp-3*, and *npp-13* (Galy *et al.*, 2003; Schetter *et al.*, 2006).

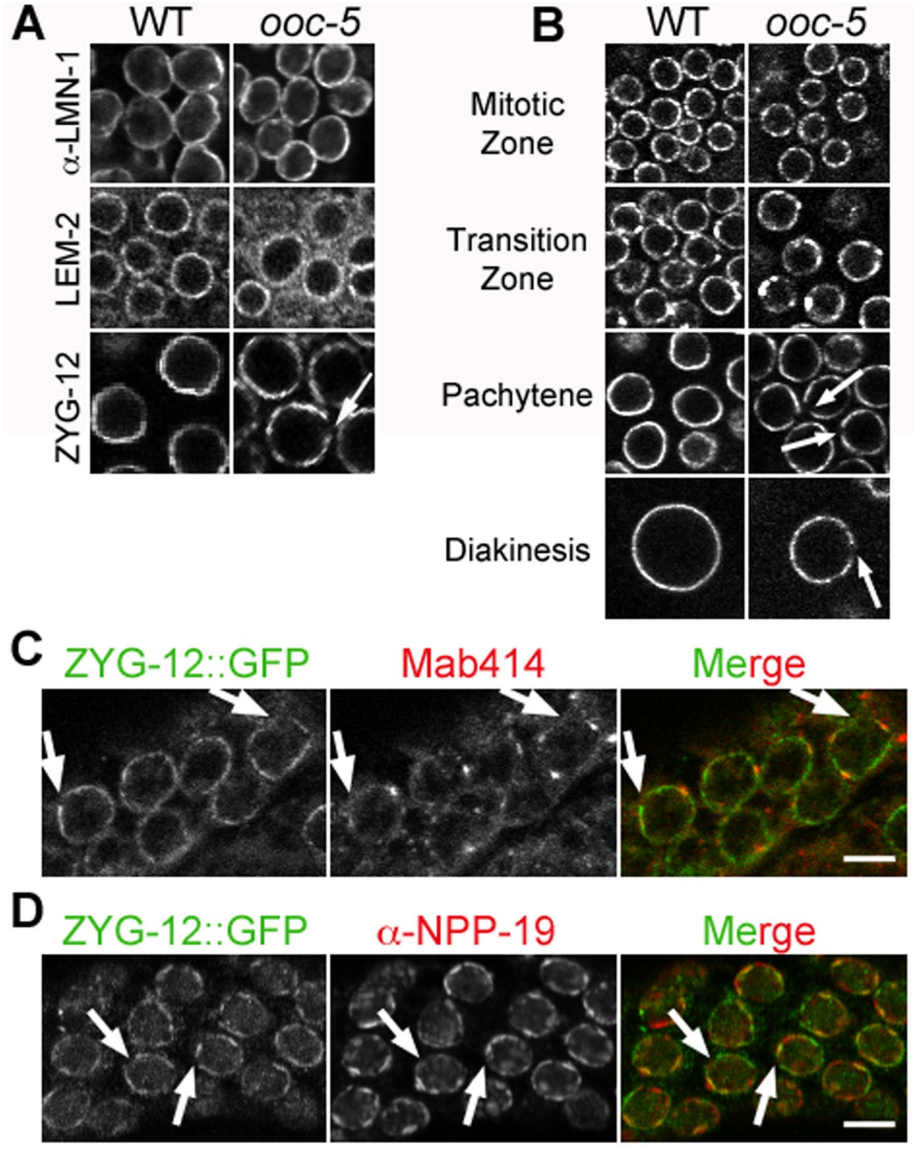

FIGURE 3: Localization of nuclear envelope–associated proteins in *ooc-5* germ cells. (A) Confocal sections of pachytene nuclei from *ooc-5* and wild-type control gonads, showing anti-lamin antibody staining or live LEM-2::GFP or ZYG-12::GFP reporter localization. (B) ZYG-12::GFP localization in different stages of gametogenesis in live worms. In *ooc-5* mutants, areas of discontinuity are seen in pachytene through diakinesis germ cell nuclei (arrows). Mab414 (C) or α-NPP-19 (D) staining of fixed *ooc-5*; ZYG-12::GFP worms. ZYG-12::GFP discontinuities that do not contain Mab414 or NPP-19 plaques are indicated (arrows). Scale bar, 5 μm.

To examine intestinal Nup phenotypes, we used a NPP-1::GFP that is expressed in the adult gut (Schetter *et al.*, 2006; Golden *et al.*, 2009). In wild-type intestinal nuclei, NPP-1::GFP outlined the entire NE, but the signal was not as continuous as in embryos or the germline, and occasional foci or streaks on the surface of nuclei were observed (Figure 4B; 12 intestines). Similar patterns were seen for other NE-associated proteins in control intestinal nuclei (Figure 4B; more than six worms each). In *ooc-5* intestinal nuclei expressing NPP-1::GFP, the NE outline was barely detectable, and multiple foci per nucleus were present (Figure 4B; $N = 13$). A similar phenotype was seen with Mab414 staining of *ooc-5* intestinal nuclei ($N = 12$). The transmembrane Nup NPP-22::GFP was more punctate in about one-half of *ooc-5(RNAi)* nuclei (Figure 4B; five worms, 6/11 nuclei) compared with controls but appeared normal in the remaining nuclei. Similarly, in 35% of nuclei stained for NPP-19, the NE outline was more punctate (Figure 4B; nine worms, 12/34 nuclei). Similar to our observations in the germline, LMN-1::YFP (Galy *et al.*, 2003) was localized normally in both *ooc-5* embryos and the intestine (embryos, $N = 6$; intestine, $N = 7$), and LEM-2::GFP was normal in *ooc-5* embryos ($N = 4$; Figure 4). Because LEM-2::GFP expression was restricted to germline and embryos, localization could not be assessed in the intestine. Together these results demonstrate that Nup mislocalization is not a germline-specific phenotype but reflects a general role for OOC-5.

Import is delayed in *ooc-5* embryos

The mislocalization of multiple nucleoporins led us to examine whether NPC functions were compromised in *ooc-5*–mutant worms. NPCs maintain a size-exclusion limit to diffusion into the nucleus, allowing small molecules to pass freely though the pore while preventing the flow of molecules >~40 kDa (Nigg, 1997). In addition, NPCs control the active transport of molecules into and out of the nucleus (D'Angelo and Hetzer, 2008). We first examined diffusion into embryonic nuclei, using GFP::tubulin (Praitis *et al.*, 2001), which has been shown to abnormally enter the nucleus in *npp-1*, *npp-3*, and *npp-13(RNAi)* embryos (Galy *et al.*, 2003; Schetter *et al.*, 2006). In wild-type embryos, GFP::tubulin was excluded from nuclei, as it is too large to freely diffuse across NPCs (~80 kDa; Figure 5A, $N = 16$). In *ooc-5* worms, GFP::tubulin was similarly excluded from embryonic nuclei (Figure 5A; $N = 16$). To validate our assay, we carried out *npp-1* RNAi on GFP::tubulin embryos and observed GFP signal inside nuclei, indicating a defect in the NPC barrier, as previously reported (Figure 5A; $N = 8$). These observations demonstrate that the barrier to passive diffusion is intact in *ooc-5* embryos.

To test further the integrity of the NPC diffusion barrier in *ooc-5*–mutant worms, we examined *ooc-5*–mutant germlines, in which the Nup phenotype is worse. We assessed the cytoplasmic and nuclear localization of fluorescein isothiocyanate (FITC)–conjugated 10-kDa dextrans and rhodamine-conjugated 70-kDa dextrans 4 h after coinjection into control and *ooc-5* germlines. In *ooc-5*/+ control worms, the 10-kDa dye was present in nuclei, whereas the 70-kDa dye was restricted to the cytoplasm, as expected (Figure 5, B and C; $N = 10$; Galy *et al.*, 2003; Updike *et al.*, 2011). After injections into *ooc-5* worms, the 70-kDa dye was similarly excluded from germline nuclei, indicating that NPCs are preventing the free diffusion of large molecules ($N = 17$). We saw a similar nuclear exclusion of GFP::tubulin from *ooc-5* germ cell nuclei, confirming our dye injection results. These results indicate that no gross defect in the NPC diffusion barrier is present in *ooc-5*–mutant worms.

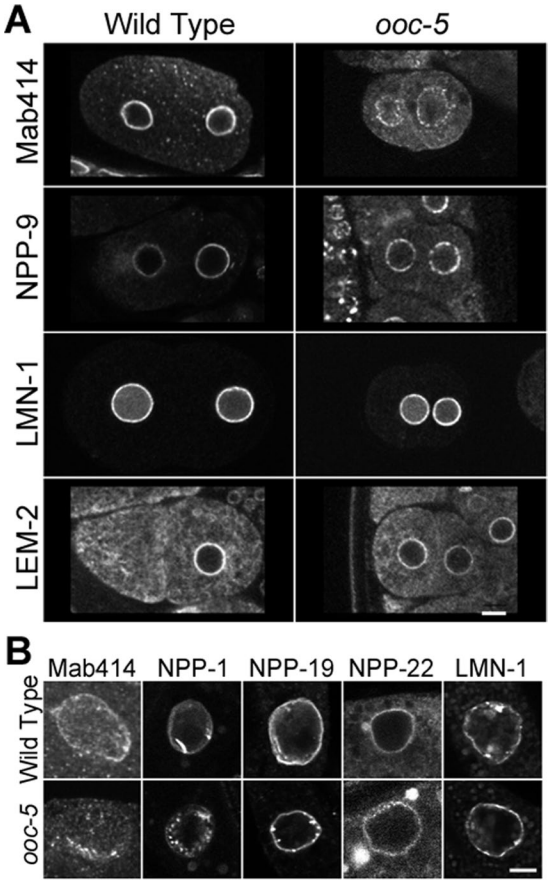

FIGURE 4: Nup mislocalization in *ooc-5* embryonic and intestinal nuclei. Confocal sections of antibody-stained and GFP-expressing live worms. (A) Fixed two-cell embryos stained for Mab414 or live two-cell embryos expressing NPP-9::GFP, LMN-1::YFP, or LEM-2::GFP reporters. (B) Intestinal nuclei stained for Mab414, anti–NPP-19, or anti–LMN-1 or expressing NPP-1::GFP or NPP-22::GFP reporters. Mab414 intestinal nuclei are *Z*-projections. Scale bars, 5 μm.

To assess nuclear transport, we examined the import of the nucleus-localized GFP reporters proliferating cell nuclear antigen (PCNA)::GFP and SUR-5::GFP (Figure 6A). PCNA::GFP is under the control of a germline promoter and expressed in germ cells and embryos, whereas SUR-5::GFP is a nuclear marker in the soma (Starr and Han, 2002; Brauchle *et al.*, 2003). SUR-5::GFP nuclear localization was similar in *ooc-5* and wild-type intestinal nuclei (15 worms each). In the germline, PCNA::GFP nuclear accumulation was detectable in pachytene and later germ cell nuclei in *ooc-5* as in wild type (*ooc-5*, nine germlines; wild type, seven germlines). PCNA::GFP was also present in *ooc-5* nuclei from one- to four-cell embryos (22 embryos). Together these results show that, despite Nup mislocalization, *ooc-5* NPCs are competent for import, at least for these specific substrates.

After NPP-1 depletion by RNAi, import of PIE-1::GFP failed in one- and two-cell embryos even though PCNA import was normal (Schetter *et al.*, 2006). We therefore assayed nuclear import of PIE-1::GFP in *ooc-5*–mutant embryos. PIE-1::GFP was enriched in the paternal pronucleus and the nuclei of the posterior cells in two- and four-cell embryos (P1 and P2, respectively), as reported (Figure 6B; $N = 16$; Mello *et al.*, 1996; Reese *et al.*, 2000). Although PIE-1::GFP was present in the posterior nucleus of the majority of *ooc-5* one- to four-cell embryos, >20% of *ooc-5* embryos failed to import PIE-1::GFP at one of these stages (8/38; Figure 6B).

Because of this partial import failure, we used time-lapse video microscopy to assess the import kinetics of PIE-1::GFP in two-cell *ooc-5* embryos. When import did occur, PIE-1::GFP took longer to become enriched in P1 nuclei in *ooc-5* compared with wild type (Figure 6C; wild type, 2.2 ± 1.6 min, $N = 8$; *ooc-5*, 4.6 ± 1.0 min, $N = 15$). Although the cell cycle was slower in *ooc-5* embryos compared with normal (wild type, 15.4 ± 1.1 min, $N = 5$; *ooc-5*, 23.5 ± 3.7 min, $N = 12$), there was not a strict correlation between cell cycle length and PIE-1::GFP import time among *ooc-5* embryos for which the movie captured the entire P1 cell cycle (Figure 6D; $N = 10$). In addition, two embryos that failed to import PIE-1::GFP in P1 nonetheless underwent division within the normal time range for *ooc-5* embryos.

Our finding of an import delay for PIE-1::GFP in embryos led us to reexamine the import of PCNA::GFP to determine whether a similar delay was occurring. Whereas all *ooc-5* embryos successfully imported PCNA::GFP into the nucleus, we found that kinetics was delayed when compared with wild-type embryos (Figure 6E; wild type, 4.8 ± 1.5 min, $N = 9$; *ooc-5*, 9.0 ± 1.5 min, $N = 5$). Kinetic assays were not possible for the PCNA::GFP and PIE-1::GFP reporters in the germline because both reporters are already present throughout the germline. Nonetheless, we observed that oocyte nuclei in the germline and embryonic nuclei were smaller in *ooc-5* compared with controls (Figure 6F). Reduced nuclear import has been shown to result in smaller nuclei in cells (D'Angelo *et al.*, 2006). Thus together our data suggest that the loss of OOC-5 results in altered nuclear import kinetics, a functional phenotype not previously reported for torsin mutants.

Ultrastructural defects in *ooc-5* NE

Disruptions of torsins in mice and *Drosophila* cause ultrastructural defects of the nuclear membrane. These defects are characterized by the accumulation of vesicle-like structures that extend from the inner nuclear membrane and protrude into the perinuclear space, producing NE "blebs" that evaginate into the cytoplasm (Goodchild *et al.*, 2005; Jokhi *et al.*, 2013; Liang *et al.*, 2014). We analyzed NE ultrastructure using EM to determine whether similar abnormalities occur in *ooc-5* mutants. We examined lengthwise sections of whole worms, allowing us to inspect the nuclear morphology of maturing germline cells within the somatic gonad, as well as nuclei in the nearby intestine and embryos inside the uterus.

In control pachytene nuclei, the ONM and INM were often visible as two thin, closely juxtaposed lines encircling the nucleus (71 nuclei). In *ooc-5* pachytene nuclei, regions of the ONM and INM were evenly spaced as in controls, although often the spacing appeared larger. However, *ooc-5* nuclei also exhibited regions with larger separations where the ONM appeared to protrude out into the cytoplasm (Figures 7 and 8 and Supplemental Figure S2). Furthermore, round, vesicle-like structures were seen within these blebs. In cross sections of pachytene nuclei, the majority of nuclei exhibited at least one bleb (Table 1). *ooc-5* diakinesis oocytes also had blebs, which were not seen in control oocytes. Most *ooc-5* oocytes had multiple blebs per nucleus and multiple vesicle-like structures per bleb, suggesting that the defect was more severe in later-stage germ cell nuclei (Table 1). *ooc-5* intestinal nuclei also had NE blebs with vesicle-like structures in the perinuclear space, similar to germline nuclei (Figure 7). Interestingly, *ooc-5* embryos, which have a less severe Nup mislocalization phenotype, did not have the large bleb phenotype (Supplemental Figure S3). Together these data

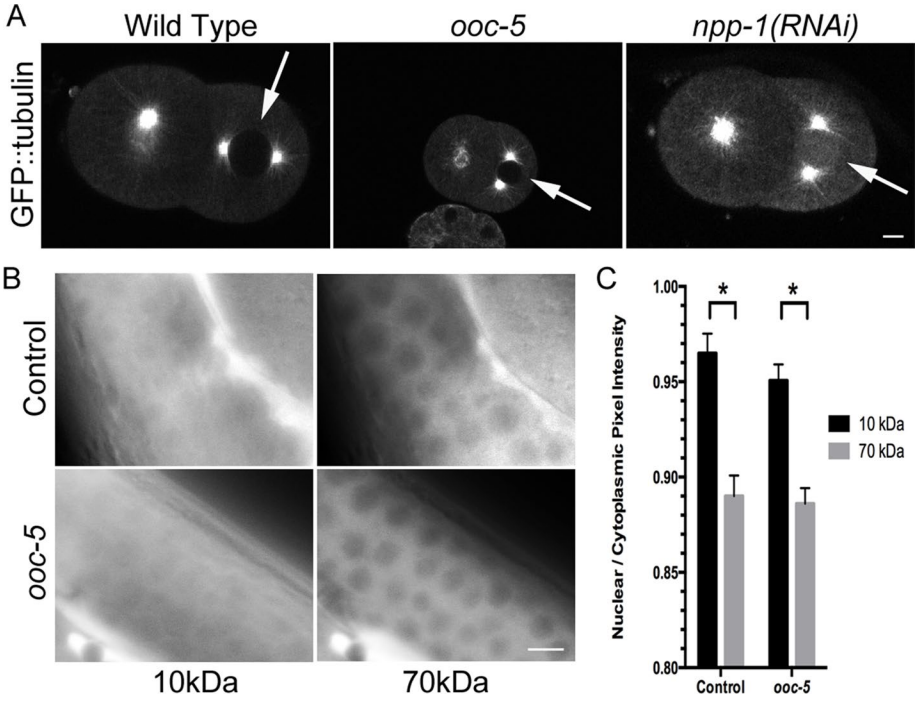

FIGURE 5: NE barrier functions are intact in *ooc-5*. (A) Confocal images of GFP::tubulin–expressing two-cell embryos at late prophase. Arrows indicate nuclei. GFP::tubulin also labels centrosomes; the failure of the P1 spindle to align on the longitudinal axis of both *ooc-5* and *npp-1*(*RNAi*) embryos is apparent. (B) A 10-kDa dye injected into wild-type or *ooc-5* gonads freely diffuses into nuclei, whereas 70-kDa dye is excluded from both wild-type and *ooc-5* germline nuclei, seen in wide-field images. Scale bars, 5 μm. (C) Quantification of dextran injection data shown in B. $*p < 1.0 \times 10^{-8}$ by paired Student's t test.

show that the role of torsin in maintaining NE ultrastructure is conserved in *C. elegans*.

Nup plaques are not localized to NE blebs

We next asked where Nup plaques are localized relative to the NE blebs seen by EM. We took advantage of the fact that P-granules are localized to clusters of NPCs in *C. elegans* pachytene nuclei and that P-granules are readily identifiable by EM at high magnification (Pitt *et al.*, 2000). P-granules are large RNPs that contain proteins and RNAs needed for both embryogenesis and subsequent germline development. In the adult germline, P-granules are associated with groups of NPCs, and these sites are believed to be the primary location for mRNA export (Pitt *et al.*, 2000; Sheth *et al.*, 2010; Updike *et al.*, 2011). Using Mab414 staining in PGL-1::GFP worms, a component of P-granules (Wolke *et al.*, 2007), we confirmed that P-granules are always colocalized to Mab414 foci in control worms (Figure 8A; 30 nuclei). In EM images of control worms, we observed juxtaposed INM and ONM membranes underneath P-granules, as expected for clusters of NPCs (Figure 8, B and C; 58 P-granules from 20 nuclei). In *ooc-5* germlines, PGL-1::GFP localized to abnormal plaques at the NE. PGL-1::GFP always colocalized with Mab414 plaques and was never localized to separate foci (Figure 8D; 46 nuclei). At the EM level, all visible P-granules were associated with areas of the NE that exhibited a juxtaposed INM and ONM, just as in wild type (Figure 8, E and F). Of importance, none of the P-granules overlaid NE blebs (0/14 P-granules from 11 nuclei) and were only occasionally adjacent to the blebs (5/14 P-granules). Together these data show that in *ooc-5* pachytene nuclei, P-granules are associated with Mab414 Nup plaques but not blebs.

DISCUSSION

Using *C. elegans* as a model, we identified novel roles for the torsin protein OOC-5 in nuclear pore localization and function. Loss of OOC-5 caused the mislocalization of multiple Nups in several tissues and abnormalities of import kinetics of two reporter proteins. Torsin proteins are known to localize to the NE, interact with integral membrane NE proteins, and disrupt NE membrane architecture, but this is the first report demonstrating roles for a torsin protein in nucleoporin localization and import.

Given the observations of delayed import kinetics and Nup mislocalization in *ooc-5* mutants, an appealing model is that OOC-5 interacts with Nups directly—for example, in nuclear pore spacing or assembly. Depletion of several different Nups causes clustering of NPCs in *C. elegans* embryos, yeast, and mammalian cell culture (Bucci and Wente, 1998; Ryan and Wente, 2002; Cohen *et al.*, 2003; Galy *et al.*, 2003; Talamas and Hetzer, 2011), although the mechanism of nuclear pore spacing is not clearly understood. Further, during interphase, NPCs assemble into the NE via a different, although unclear, mechanism compared with pore insertion after mitosis (Doucet and Hetzer, 2010; Doucet *et al.*, 2010; Dultz and Ellenberg, 2010). The observations that the Nup mislocalization phenotype is more severe in postmitotic germline and intestinal cells than in dividing embryos are consistent with a defect in some aspect of nonmitotic NPC assembly or maintenance. Interestingly, the NE structural blebs were also only present in these nondividing cell types. Torsins behave as luminal ER/NE proteins (Cookson and Clarimon, 2005; Granata *et al.*, 2009), and thus OOC-5 would be predicted to interact with transmembrane Nups. Transmembrane Nups appear to be partially redundant for functions in NPC assembly in multiple organisms; *C. elegans* has two transmembrane Nups, NPP-22 (mNdc1) and NPP-12 (mGP210). Surprisingly, the transmembrane Nup NPP-22::GFP was localized more normally in *ooc-5*–mutant germlines and intestinal cells than were peripheral Nups identified by Mab414. Thus it seems unlikely that OOC-5 acts directly on this transmembrane Nup. However, we cannot rule out an interaction between OOC-5 and NPP-12, which we were not able to analyze in *ooc-5*–mutant germlines for technical reasons.

Mislocalization of Nups in *ooc-5* mutants could also be downstream of disruptions in a newly proposed megaRNP budding pathway characterized in *Drosophila* (Speese *et al.*, 2012). MegaRNPs that form in the nucleus bud through the INM, forming transient vesicles in the perinuclear space that subsequently fuse with the ONM in a manner reminiscent of herpes virus nuclear egress (Speese *et al.*, 2012). This transport is believed to be distinct from nuclear pore export. The presence of INM evaginations and vesicle-like structures in the perinuclear space in *Drosophila* torsin mutants, together with the accumulation of ATP-locked torsin at the bud necks of wild-type megaRNP buds, led the authors to propose that torsin is required for the abscission of the buds into the perinuclear space (Jokhi *et al.*, 2013). Whether the NE abnormalities observed in *Drosophila* torsin mutants were correlated with changes in NPCs was not tested.

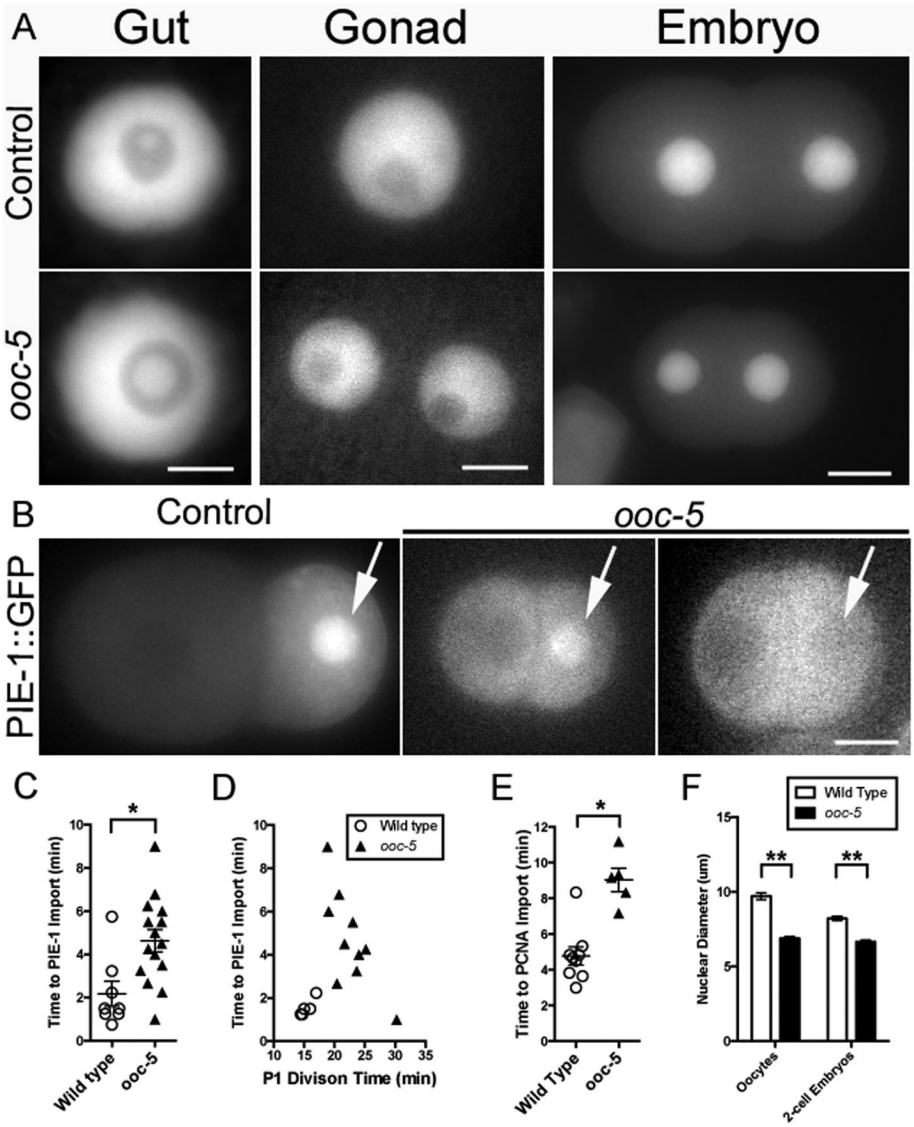

FIGURE 6: Import is delayed in *ooc-5* embryos. (A) Wide-field images showing the nuclear localization of reporters in the gut (SUR-5::GFP), gonad (PCNA::GFP), and embryos (PCNA::GFP). The light circles in the gut and gonad nuclei denote the nucleolus. (B) PIE-1::GFP is enriched only in the nucleus of the posterior, P1 cell in controls. Examples of both successful and failed import in *ooc-5* embryos are shown. Arrows point to the P1 nuclei. (C) Quantification of the time to P1 nuclear enrichment of PIE-1::GFP as measured from the onset of cytokinesis. (D) Dot plot of the time to P1 nuclear enrichment of PIE-1::GFP vs. P1 cell cycle length for wild-type and *ooc-5* embryos. (E) Quantification of the time to nuclear import of PCNA::GFP from nuclear envelope breakdown. (F) Measurement of nuclear diameters in wild-type and *ooc-5* oocytes and two-cell embryos. Scale bars, 5 μm (A, intestine and gonad), 10 μm (A, embryo; B). *$p < 0.01$ (C, E), by Student's *t* test; **$p < 1 \times 10^{-11}$ (F), by Student's *t* test.

The NE ultrastructural abnormalities identified in *Drosophila* torsin mutants are similar to those described here for *ooc-5* mutants, raising the possibility that NE budding occurs in *C. elegans*. This is intriguing because *ooc-5* was first identified for its role in embryonic polarity (Basham and Rose, 1999), and wild-type *Drosophila* megaRNPs contain homologues of the *C. elegans* anterior polarity complex, Baz/PAR-3 and aPKC/PKC-3, as well as *par-6* mRNA (Speese *et al.*, 2012). On the other hand, whereas torsin mutations in flies, *C. elegans*, and mice cause nuclear membrane evaginations into the perinuclear space, the megaRNP intermediates observed in wild-type flies invaginate into the nucleoplasm. In addition to NE invaginations at the EM level, wild-type *Drosophila* megaRNP intermediates were associated with circles of laminC localization seen by light microscopy (Jokhi *et al.*, 2013). We did not observe either NE invaginations or lamin circles in control worms. In intestinal nuclei, occasional lamin foci or streaks were present at the NE in both wild-type and *ooc-5* worms (Figure 4B), although these foci/streaks may instead reflect invaginations of the NE as part of a nucleoplasmic reticulum (Malhas *et al.*, 2011). Further studies are required to determine whether megaRNP budding through the NE occurs in *C. elegans* and whether it is linked to torsin function.

A third model to explain the Nup localization defects observed in *ooc-5* mutants is that they are a secondary effect caused by loss of OOC-5 interactions with other NE proteins. Human torsinA interacts with SUN and KASH proteins, and SUN1 has been implicated specifically in interphase pore insertion in cell culture (Talamas and Hetzer, 2011). Further, disruption of SUN1 function in HeLa cells causes NPC clustering and altered nuclear shape (Liu *et al.*, 2007). Of importance, this model is not mutually exclusive with the others discussed. Because Nup plaques in the germline are not colocalized with either discontinuities in the KASH protein ZYG-12 or NE blebs, these phenotypes may arise in parallel. Moreover, the role for OOC-5 in nuclear import shown here appears to be independent of NE blebs and any proposed functions in megaRNP budding, since no NE structural abnormalities were observed in *ooc-5* embryos. Thus, given the interactions identified to date and the results reported here, we speculate that torsins have multiple roles at the NE. Additional studies are needed to tease apart the relationships between, and functional consequences of, the multiple NE phenotypes in *ooc-5* mutants.

Although the cell types analyzed in this study are distinct from the neurons affected in DYT1 dystonia patients and torsinA-null mice, the NE structural defects are strikingly similar (Goodchild *et al.*, 2005; Jokhi *et al.*, 2013). Thus our finding of delayed import in *ooc-5* embryos could be relevant to understanding the cellular defects caused by human torsin mutations. TorsinA phenotypes in mice are restricted to neurons, likely due to considerably higher expression levels of torsinB in nonneuronal tissues (Kim *et al.*, 2010). *C. elegans* has two additional torsins, TOR-1 and TOR-2. The presence of strong Nup and NE structural phenotypes in *ooc-5* mutants argues against OOC-5 redundancy with other torsins in the tissues we examined, although it is possible that expression of TOR-1 or TOR-2 could account for the observation of only subtle import defects in *ooc-5* worms. However, published data do not indicate the expression of either TOR-1 or TOR-2 in the germline, embryos, or intestine (Cao *et al.*, 2005; Frederic *et al.*, 2013). Future work using

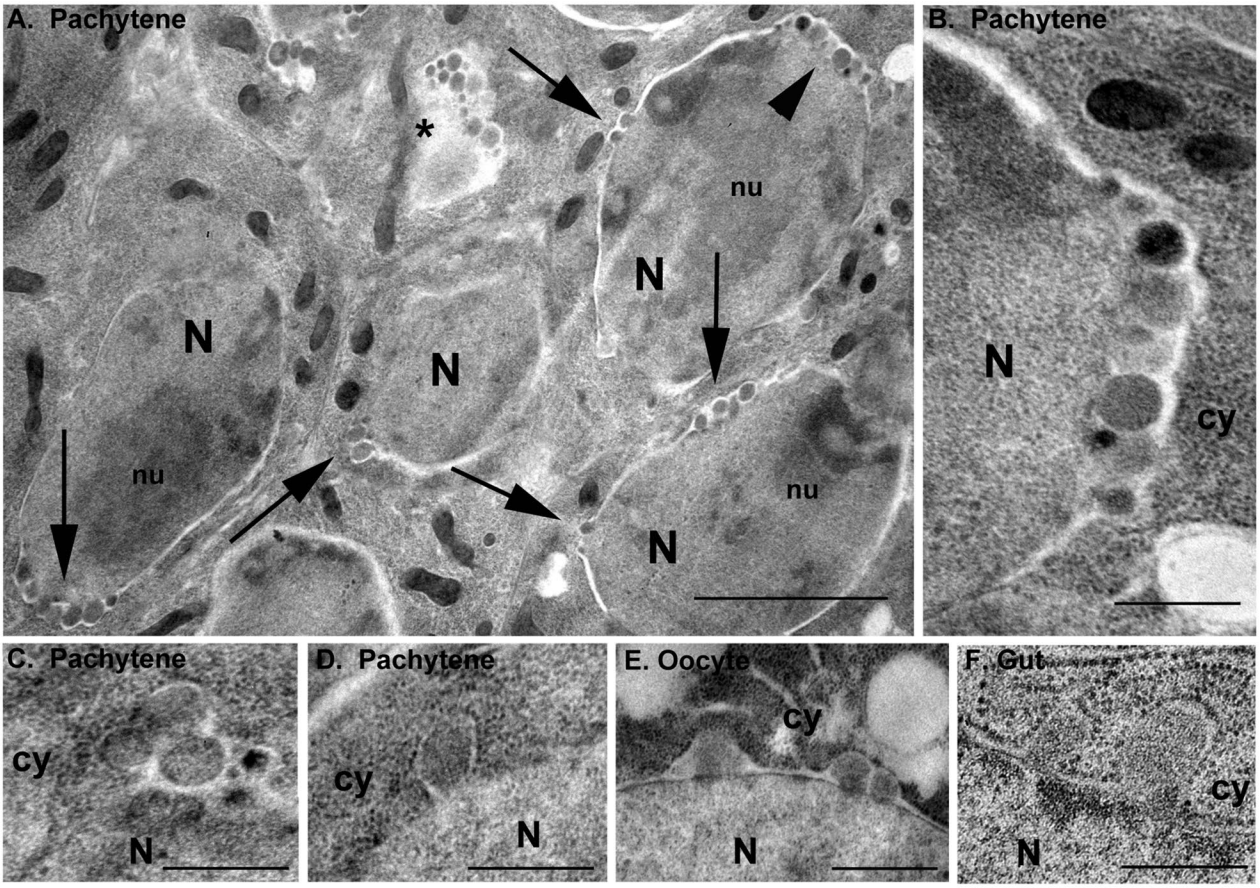

FIGURE 7: Ultrastructural defects in *ooc-5* nuclear envelopes. (A) Low magnification of *ooc-5*–mutant pachytene nuclei, showing multiple nuclei with defects (arrows). Asterisk is a tangential section through a bleb. Arrowhead points to the region magnified in B. (B–F) High magnification of blebs on *ooc-5*–mutant pachytene (B–D), oocyte (E), and intestinal (F) nuclei. Scale bar, 2 μm (A), 400 nm (B–E).

cell-specific markers is needed to determine whether loss of OOC-5 or other torsins results in Nup mislocalization or NE abnormalities in *C. elegans* neurons or other cell types. Nevertheless, because the *DYT1* ΔE mutation impairs torsinA function (Goodchild *et al.*, 2005; Zhao *et al.*, 2013; Liang *et al.*, 2014) and the strong *it145 ooc-5* allele is a known loss-of-function allele (Basham and Rose, 2001), studies of OOC-5 in *C. elegans* can serve as a valuable model for torsin function.

MATERIALS AND METHODS

Worm strains and growth

Worms were maintained according to standard protocols (Brenner, 1974; Church *et al.*, 1995). A complete list of strains is given in Supplemental Table S1.

Immunostaining

The immunostaining protocol was modified from Phillips *et al.* (2009). Worms were dissected in 15 μl EBT (egg buffer [25 mM 4-(2-hydroxyethyl)-1-piperazineethanesulfonic acid, pH 7.4, 120 mM NaCl, 48 mM KCl, 2 mM $CaCl_2$, 2 mM $MgCl_2$] + 0.1% Tween) on poly-L-lysine–coated slides. A 15-μl amount of 2% paraformaldehyde in EBT was added, and tissue was fixed for 4 min at room temperature before adding coverslips. Slides were freeze cracked and fixed in 100% methanol at −20°C for 2 min, followed by two 10-min washes in phosphate-buffered saline/0.1% Tween (PBS-T). Slides were blocked for 15 min (0.7% bovine serum albumin in PBS-T) at room temperature and then incubated in primary antibody diluted in PBS overnight at 4°C in a humidified chamber. Slides were washed 3× 10 min in PBS-T, incubated in secondary antibody diluted in PBS-T for 1 h at room temperature, and washed 2× 10 min in PBS-T and 1× 10 min in PBS. After a 2-min incubation in 4′,6-diamidino-2-phenylindole (DAPI) diluted in PBS, slides were washed 1× 10 min in PBS and mounted with VectaShield mounting medium (Vector Laboratories, Burlingame, CA). Slides were imaged on an Olympus FV1000 Laser Scanning Confocal microscope with a 60× objective.

The following primary antibodies were used: mouse monoclonal Mab414 (1:1000; Covance, Emeryville, CA), rabbit anti–NPP-19 (1:200; OWYL; Rodenas *et al.*, 2009), and guinea pig anti–LMN-1 (1:1000; Kelly Liu, Cornell University, Ithaca, NY). Rhodamine–anti-mouse, Cy3–anti-guinea pig, FITC–anti-rabbit, and Alexa 594–anti-rabbit secondary antibodies (Jackson ImmunoResearch, West Grove, PA) were used at 1:200.

Reporter strain imaging

GFP reporter worms were immobilized in 2 mM levamisole in M9 buffer on 2% agar pads and imaged live either by confocal microscopy as described or on an Olympus BX60 compound microscope using a PlanApo N 60×, 1.42 numerical aperture objective, Hamamatsu Orca 12-bit digital camera, and OpenLab software. To quantify Nup plaques, fields containing ~10 nuclei were counted for the presence or absence of Nup plaques, as well as the number of plaques per nucleus, in at least six worms per strain. To determine germ cell stages

	Control		*ooc-5*		
	Percentage blebs[a]	Nuclei (worms)	Percentage blebs[a]	Average blebs/nuclear slice[b]	Nuclei (worms)
Pachytene	0.0	71 (5)	87.9	2.8	91 (5)
Oocytes	0.0	3 (2)	100.0	9.4	14 (4)
Embryos	0.0	25 (5)	0.0	0.0	17 (2)
Gut	0.0	5 (4)	100.0	10.1	10 (2)

[a]Nuclei were scored as having a bleb if there was at least one vesicle >100 nm in diameter in a local separation of the NE.
[b]Blebs were counted in a single thin section for each nucleus that had at least one bleb.

TABLE 1: EM data summary.

in NPP-9::GFP worms, worms were fixed in 100% methanol and mounted in 2 µg/ml DAPI in M9 buffer. Nuclear diameters were measured from confocal images using ImageJ software, and an unpaired Student's *t* test was used to compare wild type and *ooc-5*.

Images of live GFP::tubulin–expressing embryos were taken by confocal microscopy as described. Exclusion of soluble GFP::tubulin from nuclei was confirmed by measuring the nuclear-to-cytoplasmic ratio of background-subtracted fluorescence intensity before NE breakdown in mitosis, when both centrosomes were clearly visible on opposite sides of the nucleus. Embryos were monitored by bright-field microscopy to ensure that images were taken before NE breakdown. Import of PCNA::GFP and PIE-1::GFP was assessed by time-lapse video microscopy. Dissected embryos were suspended in a hanging drop of egg buffer on coverslips and imaged using an Olympus BX60 compound microscope as described. Using OpenLab software, images were captured every 10 s for PCNA::GFP and every 15 s for PIE-1::GFP. For PIE-1::GFP, time to P1 nuclear enrichment was measured from the completion of the first cytokinesis to the time that the nuclear-to-cytoplasmic ratio of background-subtracted fluorescence intensity was ≥1.2. Cell cycle lengths were measured from the completion of the first cytokinesis to the completion of P1 cytokinesis. For PCNA::GFP, time to import was measured from NE breakdown in P0 to the time that the nuclear-to-cytoplasmic ratio of background-subtracted fluorescence intensity was ≥1.3 in both the AB and P1 cells. An unpaired Student's *t* test was used to compare wild-type and *ooc-5* import times.

RNA interference

The majority of the *ooc-5* coding sequence was PCR amplified and cloned into the RNAi feeding vector L4440. The *npp-1* RNAi

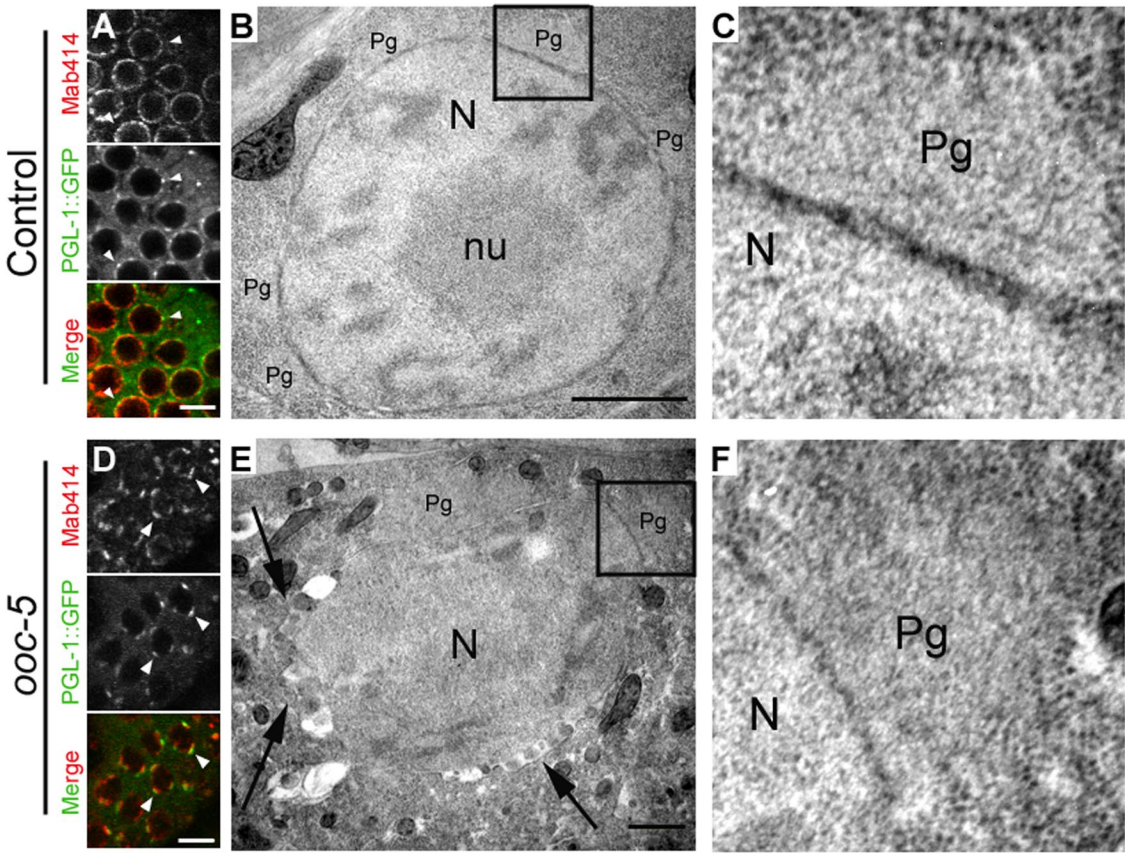

FIGURE 8: Nup plaques are not associated with NE blebs. Confocal sections of fixed germlines expressing PGL-1::GFP stained with Mab414 (A, D). Colocalization of P-granules with NPCs (arrowheads). Electron microscopy of a pachytene nucleus with P-granules labeled from control (B) and *ooc-5* (E) worms. Blebs in *ooc-5* are marked with arrows. (C, F) High magnification of the boxed regions. Scale bars, 5 µm (A, D), 400 nm (B, E). N, nucleus; nu, nucleolus; Pg, P-granules.

feeding construct was from the Ahringer library, clone IV-5K01 (Kamath *et al.*, 2003). L4 larvae were picked onto bacteria expressing double-stranded RNA and incubated at 23°C. *npp-1(RNAi)* embryos were examined after 48 h. For *ooc-5(RNAi)*, only surviving worms from the next generation that had a double row of oocytes in the proximal gonad were subsequently analyzed.

Electron microscopy

Young adult nematodes were prepared for transmission electron microscopy by high-pressure freezing and freeze substitution following standard methods for ultrastructure (Hall *et al.*, 2012). *unc-4(e120)* worms served as controls. After embedding into plastic resin, lengthwise thin sections were collected with a RMC Powertome (Boeckler Instruments, Tucson, AZ) onto Formvar-coated slot grids for inspection with a Philips CM10 electron microscope. Digital images were collected with an Olympus SIS Morada camera system and analyzed using iTEM software and Photoshop. Montages of low-power images were used to document the layout of tissues in each animal, and then higher-power images were used to determine the morphology of the nuclear membrane and localization of P-granules. All quantification was done on individual cross-sectional images of nuclei.

Dextran dye injections

Young adult worms were coinjected with fluorescent dextrans (Sigma-Aldrich, St. Louis, MO) as described previously (Schetter *et al.*, 2006; Updike *et al.*, 2011). FITC-conjugated 10-kDa dextran (0.25 mg/ml) and rhodamine-conjugated 70-kDa dextran (1 mg/ml) in injection buffer (20 mM KPO_4, pH 7.5, 3 mM potassium citrate, 2% polyethylene glycol) were used. After 4 h of recovery at room temperature (~23°C), worms were immobilized in 2 mM levamisole in M9 buffer on 2% agar pads and imaged live on an Olympus BX60 compound microscope. Exclusion of dextrans was quantified by measuring the nuclear-to-cytoplasmic ratio of background-subtracted fluorescence intensity in multiple nuclei from each gonad. The same nuclei were used for measuring both 10- and 70-kDa fluorescence. A paired Student's *t* test was used to compare 10- kDa exclusion to 70-kDa exclusion.

ACKNOWLEDGMENTS

We thank Sumati Hasani for assistance in generating strains, members of the Rose lab for technical help, and Leslie Gunther and Geoff Perumal for help with high-pressure freeze fixations. We are grateful to Geraldine Seydoux (Johns Hopkins University School of Medicine, Baltimore, MD), Orna Cohen-Fix (National Institute of Diabetes and Digestive and Kidney Diseases, Bethesda, MD), Anne Spang (University of Basel, Basel, Switzerland), and Dan Starr (University of California, Davis, Davis, CA) for generously providing strains. Some strains were provided by the *Caenorhabditis* Genetics Center, which is funded by the National Institutes of Health Office of Research Infrastructure Programs (P40 OD010440). We also thank Peter Askjaer (European Molecular Biology Laboratory, Heidelberg, Germany) for anti–NPP-19 antibody and Kelly Liu (Cornell University, Ithaca, NY) for anti-lamin antibody. M.J.W.V. and L.S.R. were supported by the Dystonia Medical Research Foundation and National Institutes of Health Grant 1R01GM68744. M.J.W.V. was also supported by National Institutes of Health Grant 1F32GM103041, W.T.D. received support from National Institutes of Health Grant 1R01NS077730, and D.H.H. and K.C.Q.N. received support from National Institutes of Health Grant OD 010943.

REFERENCES

Basham SE, Rose LS (1999). Mutations in *ooc-5* and *ooc-3* disrupt oocyte formation and the reestablishment of asymmetric PAR protein localization in two-cell *Caenorhabditis elegans* embryos. Dev Biol 215, 253–263.

Basham SE, Rose LS (2001). The *Caenorhabditis elegans* polarity gene *ooc-5* encodes a Torsin-related protein of the AAA ATPase superfamily. Development 128, 4645–4656.

Brauchle M, Baumer K, Gonczy P (2003). Differential activation of the DNA replication checkpoint contributes to asynchrony of cell division in *C. elegans* embryos. Curr Biol 13, 819–827.

Brenner S (1974). The genetics of Caenorhabditis elegans. Genetics 77, 71–94.

Bucci M, Wente SR (1998). A novel fluorescence-based genetic strategy identifies mutants of Saccharomyces cerevisiae defective for nuclear pore complex assembly. Mol Biol Cell 9, 2439–2461.

Caldwell GA, Cao S, Sexton EG, Gelwix CC, Bevel JP, Caldwell KA (2003). Suppression of polyglutamine-induced protein aggregation in Caenorhabditis elegans by torsin proteins. Hum Mol Genet 12, 307–319.

Cao S, Gelwix CC, Caldwell KA, Caldwell GA (2005). Torsin-mediated protection from cellular stress in the dopaminergic neurons of Caenorhabditis elegans. J Neurosci 25, 3801–3812.

Chen P, Burdette AJ, Porter JC, Ricketts JC, Fox SA, Nery FC, Hewett JW, Berkowitz LA, Breakefield XO, Caldwell KA, Caldwell GA (2010). The early-onset torsion dystonia-associated protein, torsinA, is a homeostatic regulator of endoplasmic reticulum stress response. Hum Mol Genet 19, 3502–3515.

Church DL, Guan KL, Lambie EJ (1995). Three genes of the MAP kinase cascade, mek-2, mpk-1/sur-1 and let-60 ras, are required for meiotic cell cycle progression in Caenorhabditis elegans. Development 121, 2525–2535.

Cohen M, Feinstein N, Wilson KL, Gruenbaum Y (2003). Nuclear pore protein gp210 is essential for viability in HeLa cells and Caenorhabditis elegans. Mol Biol Cell 14, 4230–4237.

Cookson MR, Clarimon J (2005). Dystonia and the nuclear envelope. Neuron 48, 875–877.

D'Angelo MA, Anderson DJ, Richard E, Hetzer MW (2006). Nuclear pores form de novo from both sides of the nuclear envelope. Science 312, 440–443.

Dauer W (2014). Inherited isolated dystonia: clinical genetics and gene function. Neurotherapeutics 11, 807–816.

Davis LI, Blobel G (1987). Nuclear pore complex contains a family of glycoproteins that includes p62: glycosylation through a previously unidentified cellular pathway. Proc Natl Acad Sci USA 84, 7552–7556.

Doucet CM, Hetzer MW (2010). Nuclear pore biogenesis into an intact nuclear envelope. Chromosoma 119, 469–477.

Doucet CM, Talamas JA, Hetzer MW (2010). Cell cycle-dependent differences in nuclear pore complex assembly in metazoa. Cell 141, 1030–1041.

Dultz E, Ellenberg J (2010). Live imaging of single nuclear pores reveals unique assembly kinetics and mechanism in interphase. J Cell Biol 191, 15–22.

D'Angelo MA, Hetzer MW (2008). Structure, dynamics and function of nuclear pore complexes. Trends Cell Biol 18, 456–466.

Frederic MY, Lundin VF, Whiteside MD, Cueva JG, Tu DK, Kang SY, Singh H, Baillie DL, Hutter H, Goodman MB, *et al.* (2013). Identification of 526 conserved metazoan genetic innovations exposes a new role for cofactor E-like in neuronal microtubule homeostasis. PLoS Genet 9, e1003804.

Galy V, Mattaj IW, Askjaer P (2003). Caenorhabditis elegans nucleoporins Nup93 and Nup205 determine the limit of nuclear pore complex size exclusion in vivo. Mol Biol Cell 14, 5104–5115.

Gerace L (2004). TorsinA and torsion dystonia: unraveling the architecture of the nuclear envelope. Proc Natl Acad Sci USA 101, 8839–8840.

Golden A, Liu J, Cohen-Fix O (2009). Inactivation of the C. elegans lipin homolog leads to ER disorganization and to defects in the breakdown and reassembly of the nuclear envelope. J Cell Sci 122, 1970–1978.

Gonzalez-Alegre P, Paulson HL (2004). Aberrant cellular behavior of mutant torsinA implicates nuclear envelope dysfunction in DYT1 dystonia. J Neurosci 24, 2593–2601.

Goodchild RE, Dauer WT (2004). Mislocalization to the nuclear envelope: an effect of the dystonia-causing torsinA mutation. Proc Natl Acad Sci USA 101, 847–852.

Goodchild RE, Dauer WT (2005). The AAA+ protein torsinA interacts with a conserved domain present in LAP1 and a novel ER protein. J Cell Biol 168, 855–862.
Goodchild RE, Kim CE, Dauer WT (2005). Loss of the dystonia-associated protein torsinA selectively disrupts the neuronal nuclear envelope. Neuron 48, 923–932.
Gorjanacz M, Jaedicke A, Mattaj IW (2007). What can Caenorhabditis elegans tell us about the nuclear envelope? FEBS Lett 581, 2794–2801.
Granata A, Schiavo G, Warner TT (2009). TorsinA and dystonia: from nuclear envelope to synapse. J Neurochem 109, 1596–1609.
Hall DH, Hartwieg E, Nguyen KC (2012). Modern electron microscopy methods for C. elegans. Methods Cell Biol 107, 93–149.
Hanson PI, Whiteheart SW (2005). AAA+ proteins: have engine, will work. Nat Rev Mol Cell Biol 6, 519–529.
Jokhi V, Ashley J, Nunnari J, Noma A, Ito N, Wakabayashi-Ito N, Moore MJ, Budnik V (2013). Torsin mediates primary envelopment of large ribonucleoprotein granules at the nuclear envelope. Cell Rep 3, 988–995.
Jungwirth MT, Kumar D, Jeong DY, Goodchild RE (2011). The nuclear envelope localization of DYT1 dystonia torsinA-DeltaE requires the SUN1 LINC complex component. BMC Cell Biol 12, 24.
Kamath RS, Fraser AG, Dong Y, Poulin G, Durbin R, Gotta M, Kanapin A, Le Bot N, Moreno S, Sohrmann M, *et al*. (2003). Systematic functional analysis of the Caenorhabditis elegans genome using RNAi. Nature 421, 231–237.
Kim CE, Perez A, Perkins G, Ellisman MH, Dauer WT (2010). A molecular mechanism underlying the neural-specific defect in torsinA mutant mice. Proc Natl Acad Sci USA 107, 9861–9866.
Liang CC, Tanabe LM, Jou S, Chi F, Dauer WT (2014). TorsinA hypofunction causes abnormal twisting movements and sensorimotor circuit neurodegeneration. J Clin Invest 124, 3080–3092.
Liu Q, Pante N, Misteli T, Elsagga M, Crisp M, Hodzic D, Burke B, Roux KJ (2007). Functional association of Sun1 with nuclear pore complexes. J Cell Biol 178, 785–798.
Malhas A, Goulbourne C, Vaux DJ (2011). The nucleoplasmic reticulum: form and function. Trends Cell Biol 21, 362–373.
Malone CJ, Misner L, Le Bot N, Tsai MC, Campbell JM, Ahringer J, White JG (2003). The C. elegans hook protein, ZYG-12, mediates the essential attachment between the centrosome and nucleus. Cell 115, 825–836.
Mello CC, Schubert C, Draper B, Zhang W, Lobel R, Priess JR (1996). The PIE-1 protein and germline specification in C. elegans embryos. Nature 382, 710–712.
Naismith TV, Heuser JE, Breakefield XO, Hanson PI (2004). TorsinA in the nuclear envelope. Proc Natl Acad Sci USA 101, 7612–7617.
Nery FC, Armata IA, Farley JE, Cho JA, Yaqub U, Chen P, da Hora CC, Wang Q, Tagaya M, Klein C, *et al*. (2011). TorsinA participates in endoplasmic reticulum-associated degradation. Nat Commun 2, 393.
Nery FC, Zeng J, Niland BP, Hewett J, Farley J, Irimia D, Li Y, Wiche G, Sonnenberg A, Breakefield XO (2008). TorsinA binds the KASH domain of nesprins and participates in linkage between nuclear envelope and cytoskeleton. J Cell Sci 121, 3476–3486.
Nigg EA (1997). Nucleocytoplasmic transport: signals, mechanisms and regulation. Nature 386, 779–787.
Penkner AM, Fridkin A, Gloggnitzer J, Baudrimont A, Machacek T, Woglar A, Csaszar E, Pasierbek P, Ammerer G, Gruenbaum Y, Jantsch V (2009). Meiotic chromosome homology search involves modifications of the nuclear envelope protein Matefin/SUN-1. Cell 139, 920–933.
Phillips CM, McDonald KL, Dernburg AF (2009). Cytological analysis of meiosis in Caenorhabditis elegans. Methods Mol Biol 558, 171–195.
Pitt JN, Schisa JA, Priess JR (2000). P granules in the germ cells of Caenorhabditis elegans adults are associated with clusters of nuclear pores and contain RNA. Dev Biol 219, 315–333.
Praitis V, Casey E, Collar D, Austin J (2001). Creation of low-copy integrated transgenic lines in Caenorhabditis elegans. Genetics 157, 1217–1226.
Reese KJ, Dunn MA, Waddle JA, Seydoux G (2000). Asymmetric segregation of PIE-1 in C. elegans is mediated by two complementary mechanisms that act through separate PIE-1 protein domains. Mol Cell 6, 445–455.
Rodenas E, Klerkx EP, Ayuso C, Audhya A, Askjaer P (2009). Early embryonic requirement for nucleoporin Nup35/NPP-19 in nuclear assembly. Dev Biol 327, 399–409.
Ryan KJ, Wente SR (2002). Isolation and characterization of new Saccharomyces cerevisiae mutants perturbed in nuclear pore complex assembly. BMC Genet 3, 17.
Sato A, Isaac B, Phillips CM, Rillo R, Carlton PM, Wynne DJ, Kasad RA, Dernburg AF (2009). Cytoskeletal forces span the nuclear envelope to coordinate meiotic chromosome pairing and synapsis. Cell 139, 907–919.
Schetter A, Askjaer P, Piano F, Mattaj I, Kemphues K (2006). Nucleoporins NPP-1, NPP-3, NPP-4, NPP-11 and NPP-13 are required for proper spindle orientation in C. elegans. Dev Biol 289, 360–371.
Sheth U, Pitt J, Dennis S, Priess JR (2010). Perinuclear P granules are the principal sites of mRNA export in adult C. elegans germ cells. Development 137, 1305–1314.
Speese SD, Ashley J, Jokhi V, Nunnari J, Barria R, Li Y, Ataman B, Koon A, Chang YT, Li Q, *et al*. (2012). Nuclear envelope budding enables large ribonucleoprotein particle export during synaptic Wnt signaling. Cell 149, 832–846.
Starr DA, Fridolfsson HN (2010). Interactions between nuclei and the cytoskeleton are mediated by SUN-KASH nuclear-envelope bridges. Annu Rev Cell Dev Biol 26, 421–444.
Starr DA, Han M (2002). Role of ANC-1 in tethering nuclei to the actin cytoskeleton. Science 298, 406–409.
Stavru F, Hulsmann BB, Spang A, Hartmann E, Cordes VC, Gorlich D (2006). NDC1: a crucial membrane-integral nucleoporin of metazoan nuclear pore complexes. J Cell Biol 173, 509–519.
Talamas JA, Hetzer MW (2011). POM121 and Sun1 play a role in early steps of interphase NPC assembly. J Cell Biol 194, 27–37.
Tanabe LM, Kim CE, Alagem N, Dauer WT (2009). Primary dystonia: molecules and mechanisms. Nat Rev Neurol 5, 598–609.
Updike DL, Hachey SJ, Kreher J, Strome S (2011). P granules extend the nuclear pore complex environment in the C. elegans germ line. J Cell Biol 192, 939–948.
Vale RD (2000). AAA proteins. Lords of the ring. J Cell Biol 150, F13–F19.
Voronina E, Seydoux G (2010). The C. elegans homolog of nucleoporin Nup98 is required for the integrity and function of germline P granules. Development 137, 1441–1450.
Wente SR, Rout MP (2010). The nuclear pore complex and nuclear transport. Cold Spring Harb Perspect Biol 2, a000562.
Wolke U, Jezuit EA, Priess JR (2007). Actin-dependent cytoplasmic streaming in C. elegans oogenesis. Development 134, 2227–2236.
Zhao C, Brown RS, Chase AR, Eisele MR, Schlieker C (2013). Regulation of torsin ATPases by LAP1 and LULL1. Proc Natl Acad Sci USA 110, E1545–E1554.